catalysts

MDPI

Article

Mesoporous ZSM-5 Zeolites in Acid Catalysis: Top-Down vs. Bottom-Up Approach

Pit Losch [1,2], Thomas C. Hoff [3], Joy F. Kolb [1], Claire Bernardon [1], Jean-Philippe Tessonnier [3,*] and Benoît Louis [1,*]

1 Laboratoire de Synthèse Réactivité Organiques et Catalyse, Institut de Chimie, UMR 7177 CNRS, Université de Strasbourg, 1 rue Blaise Pascal, 67000 Strasbourg CEDEX, France; losch@mpi-muelheim.mpg.de (P.L.); joy.kolb@hotmail.fr (J.F.K.); claire.bernardon@gmail.com (C.B.)

2 Department of Heterogeneous Catalysis, Max-Planck-Institut für Kohlenforschung, D 45470 Mülheim an der Ruhr, Germany

3 Department of Chemical & Biological Engineering, Iowa State University, 2138 Biorenewables Research Laboratory, 617 Bissell Road, Ames, IA 50011-1098, USA; thoff@iastate.edu

* Corresponding authors: tesso@iastate.edu (J.-P.T.); blouis@unistra.fr (B.L.); Tel.: +1-515-294-4595 (J.-P.T.); +33-368851344 (B.L.)

Received: 26 May 2017; Accepted: 19 July 2017; Published: 26 July 2017

Abstract: A top-down desilication of Al-rich ZSM-5 zeolites and a bottom-up mesopores creating method were evaluated in this study. Three liquid–solid and one gas–solid heterogeneously-catalysed reactions were chosen to establish relationships between zeolites textural properties and their catalytic behavior in acid-catalysed model reactions that are influenced by shape selectivity: Diels-Alder cyclization between isoprene and methylacrylate, Methanol-to-Olefins (MTO) reaction, chlorination of iodobenzene with trichloroisocyanuric acid (TCCA), and Friedel-Crafts acylation of anisole by carboxylic acids with differing sizes. It is found amongst others that no optimal mesoporosity for all the different reactions can be easily obtained, but depending on the chosen application, a specific treatment has to be set to achieve high activity/selectivity and stability.

Keywords: zeolite; desilication; acid catalysis; mesoporosity

1. Introduction

In the past few decades, zeolites with hierarchical porosity have been reported to outperform their purely microporous counterparts in numerous acid catalysed reactions [1–4]. Usually, this behavior is assigned to improved mass transfer due to the introduction of a secondary mesoporous network of inter- or intra-crystalline nature. Indeed, hierarchically porous zeolites offer enhanced accessibility and transport of molecules to and from the active sites [5–8], therefore enhancing catalyst effectiveness [1–4,9]. It is of utmost importance to be able to characterise and to guarantee good pore connectivity in order to take benefits from those advantages [10–13].

Versatile templating and non-templating methods have been described to prepare hierarchical zeolites in the form of nanocrystals, composites, and mesoporous crystals [14–21]. Top-down approaches to introduce intracrystalline mesoporosity in zeolites are cheap and the most commonly used. The latter methods consist in the removal of framework T-atoms: Al^{3+} by steam or acid treatment (dealumination) [22], and Si^{4+} by base treatment (desilication) [23]. Particularly desilication, typically with aqueous NaOH solutions, seems attractive due to extensive mesopore formation and easy scale-up [24]. Besides NaOH, several other strong bases of inorganic (LiOH, KOH, and Na_2CO_3) or organic (TMAOH, TPAOH) nature have been used as desilicating agents to generate mesopores in zeolites [25–27].

Depending on the targeted catalytic reaction, a proper balance between drawbacks and advantages has to be set, as a case-by-case study, which may suggest that dealumination with respect to desilication could be envisaged. For instance, sequential treatments as successive dealumination-desilication-resilylation on external surfaces are proposed in the literature [28]. It has been reported that furfural selectivity was higher in dealuminated ZSM-5 zeolites than in desilicated samples [29]. Several interesting reviews cover this topic [30–33]. An important drawback, so far, is the increased difficulty to produce mesopores in Al-rich ZSM-5 zeolites using the desilication method [30].

There is a priori no general rule to select either bottom-up or top-down prepared hierarchical zeolites in terms of performance in a defined catalytic reaction. The decisive criterion remains the catalyst's production costs: It is important to note that rationally conceived bottom-up mesoporous zeolites are usually by orders of magnitude more expensive to synthesise than the earlier described desilicated ones. Indeed, ingenious organic templates (typically cationic surfactants) render these syntheses not yet applicable for large-scale industry [34]. There are, however, tendencies to replace these expensive templates by bio-sourced cheaper mesoporogens [35,36]. Thus, it remains interesting to explore and compare both routes.

In the present study, we have therefore decided to compare a top-down desilication of Al-rich ZSM-5 zeolites to a bottom-up mesopores creating approach. Several zeolites were modified by a cheap desilication post-treatment, while seeking optimum NaOH-concentration/time/temperature conditions, and compared with two mesopores-containing as-synthesised zeolites. This comparison has been carried out in terms of thorough characterisation of the materials by scanning electron microscopy (SEM), N_2 sorption measurements (BET), ammonia thermally programmed desorption (NH_3-TPD), H/D isotope labelling for Brønsted acid sites titration and elemental analysis (ICP-AES) techniques. Our study focuses on the behavior in acid catalysis of this series of zeolites. Three liquid–solid and one gas–solid heterogeneously-catalysed reactions were chosen to evaluate the importance of textural properties in the series of investigated materials. The studied reactions were: (i) the Diels-Alder cyclisation between isoprene and methylacrylate; (ii) the Methanol-to-Olefins (MTO) reaction; (iii) the chlorination of iodobenzene with trichloroisocyanuric acid (TCCA); (iv) the Friedel-Crafts acylation of anisole by two differently sized carboxylic acids. Indeed, those reactions were already shown to be influenced by either the presence of mesoporosity or hindered by the presence of defects which might be induced by desilication of the zeolites [37–40].

In addition to producing valuable bulk chemicals (MTO), fertilisers or building blocks for the pharmaceutical industry, these reactions were chosen based on the different molecular sizes involved, which may give precious hints on the pore connectivity of tested materials. Ultimately, it was aimed to extract concluding structure-activity relationships for the investigated catalysts.

2. Results

Characterisation

Table 1 presents the textural properties of all prepared and tested zeolites. Different acid site densities could be measured using different approaches: at first, a theoretical acid site density could be calculated based on Si/Al ratio. NH_3-TPD allowed the estimation of the Si-(OH)-Al linked, strong Brønsted acid sites, while the H/D isotope exchange technique quantified all exchangeable hydrons, thus including silanols and extra-framework aluminium (EFAl) related defects, which are known to interfere during acid catalysis [41]. For entries 1–4, the theoretical and indeed accessible Brønsted acid sites titrated by ammonia are in good agreement, whilst for entries 5, 7 and 8, less acid sites could be experimentally measured than theoretically predicted; and lastly, in entry 6, more acid sites are detected than predicted.

Table 1. Textural properties of the different ZSM-5 zeolites.

Zeolite	N(H$^+$) [mmol (H$^+$) g^{-1}] [a]	N(H$^+$) [mmol (H$^+$) g^{-1}] [b]	$N_{theor.}$(H$^+$) [mmol (H$^+$) g^{-1}] [c]	Si/Al Ratio	S_{BET} [m^2 g^{-1}]	S_{ext} [m^2 g^{-1}]	S_{int} [m^2 g^{-1}]
SZ-MW	1.11	0.57	0.58	26	438	254	183
SZ-CO	0.71	0.28	0.33	47	421	215	207
CBV2314	1.48	1.17	1.25	12	376	276	100
DZ-0.2M-45	1.95	1.37	1.18	12	310	264	46
DZ-0.2M-75	1.29	0.67	1.23	12	409	277	133
DZ-0.2M-105	2.80	1.47	1.11	13	413	328	85
DZ-0.5M-45	4.06	0.68	1.11	13	397	239	158
DZ-1.0M-75	1.42	0.92	1.86	8	378	262	116

Acid site densities were evaluated by different ways: [a] H/D isotope exchange measuring the total amount of exchangeable hydrons; [b] NH_3-TPD: only strong Brønsted acid sites were titrated, corresponding to Si-(OH)-Al bridging sites; [c] Theoretical acid site density based on the Si/Al ratio.

It is worthy to note that each sample exhibited a notable amount of defects-related exchangeable hydrons. Especially, entry 7 shows a dramatic amount of O-H groups (4 times superior to the theoretical value). Specific surface areas (S_{BET}) of the different zeolites indicate that the two as-synthesized zeolites (entries 1 and 2) exhibit the largest specific surface areas as well as internal porosity. For the cheaper desilicated zeolite MFI-family, it seems that a medium-strong treatment led to the highest improvement in S_{BET}, which increased by 10% from 376 to 413 m^2 g^{-1} (entries 3 compared to 6).

XRD patterns indicate that the crystalline framework is maintained even after drastic alkaline treatment (DZ-0.5M-45, entry 7, Figure S1), but suffers severely for the harshest treatment conditions (DZ-1.0M-75, entry 8, Figure 1). Furthermore, the two as-synthesised zeolites are of similar crystalline quality (periodical order of the crystallographic planes) as commercial CBV2314 zeolite.

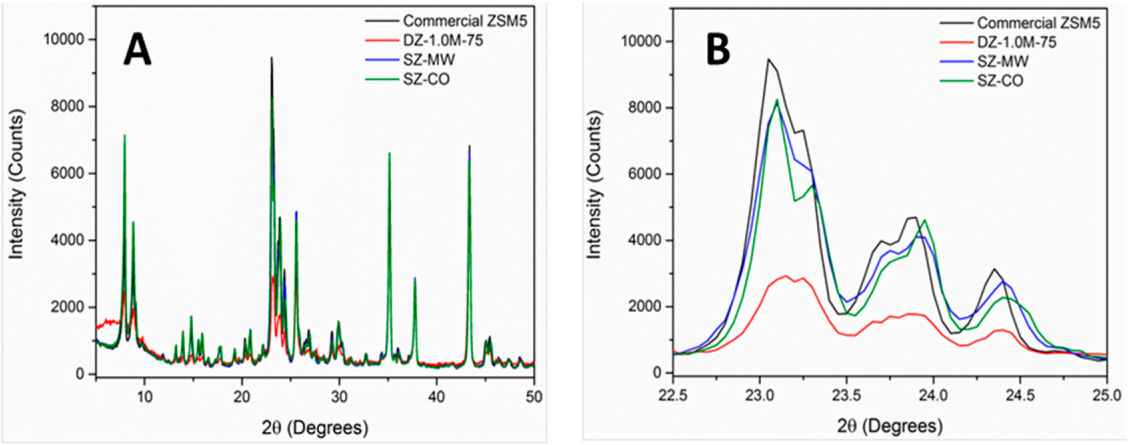

Figure 1. Powder X-ray diffraction (XRD) patterns obtained for (**A**) commercial and hierarchal zeolites (**B**) scaled to the most intense characteristic MFI peaks.

Crystalline morphologies were evaluated with SEM. SEM images, presented in Figure 2, show that the harsh treatment with NaOH (corresponding to entry 8 in Table 1) could, indeed, lead to the formation of debris, smaller crystallites and disaggregated parent crystals. Figure 2c,d, on the other hand, confirm that the two as-prepared zeolites exhibit a well-defined (probably) intercrystalline mesoporosity, as larger micron-sized aggregates are homogeneously built from 50 to 100 nm sized crystallites. Table S2 reports the micro- and mesoporous volumes. Our former study assessed the relationship between rough crystals and the presence of mesopores between the nanoparticles [38,42].

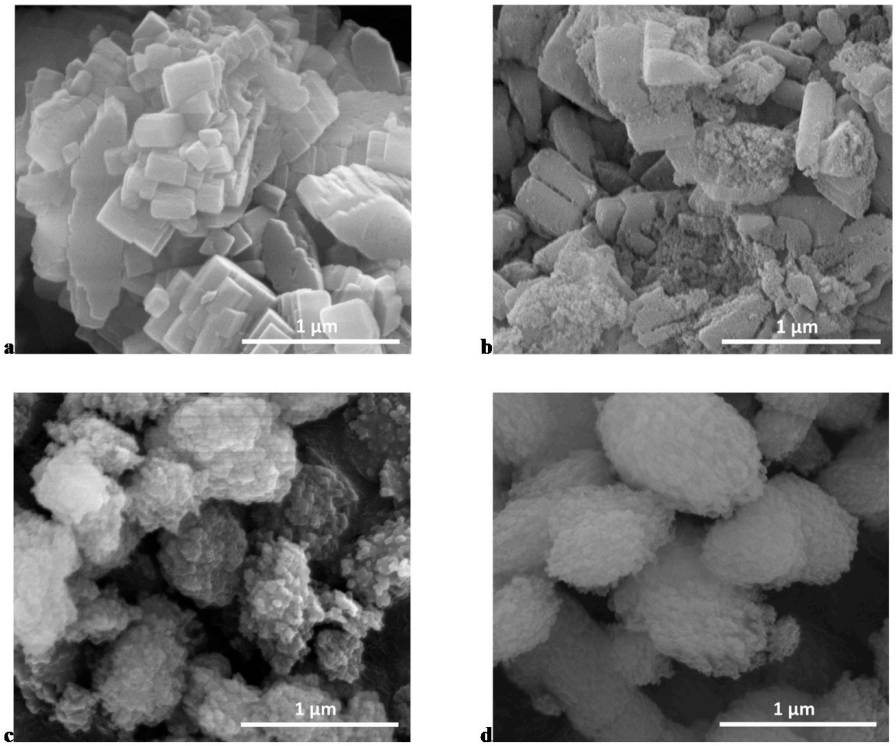

Figure 2. Scanning electron microscopy (SEM) images of (**a**) parent commercial ZSM-5 (Zeolyst International, CBV2314); (**b**) NaOH desilicated ZSM-5 (DZ-1.0M-75); (**c**) hierarchical ZSM-5 synthesised in a conventional oven; and (**d**) hierarchical ZSM-5 synthesised through microwave heating.

Further SEM images, as well as nitrogen adsorption/desorption isotherms, which cover the complete investigated series and confirm the same trends, are given in Supplementary Materials (Figures S2 and S3).

Figure 3 shows N_2 adsorption-desorption isotherms for the tested ZSM-5 zeolites and their mesopore size distributions. Interestingly, each treated and synthesised zeolite exhibits a certain amount of mesopores when compared to pristine commercial zeolite. The four presented nitrogen adsorption-desorption isotherms are of type I tending to IV (typical for micro-mesoporous materials). The four samples therefore exhibit a complex porosity, microporous and mesoporous in nature. Indeed, the hysteresis loop type IV also indicates the presence of parallel meso- and microporosity. The degree of mesopores introduction seems to be proportional to the severity of the alkaline treatment (Figure 3, Table 1). Especially, the harshly treated DZ-1.0M-75 exhibits a hysteresis loop tending to type I, indicating the presence of perfectly cylindrical mesopores (with a porous diameter of 10 nm, Figure 3b). The two as-prepared zeolites also contain a non-negligible amount of mesopores. It is important to note here, especially considering the following catalysis part, that the presence of mesopores is not the sole important parameter to respect. Indeed, a certain preservation of the initial microporous network is essential too [43]. In other terms, the connectivity between the transport-responsible mesopores and catalysis-responsible micropores is important and will be evaluated later by the catalytic results.

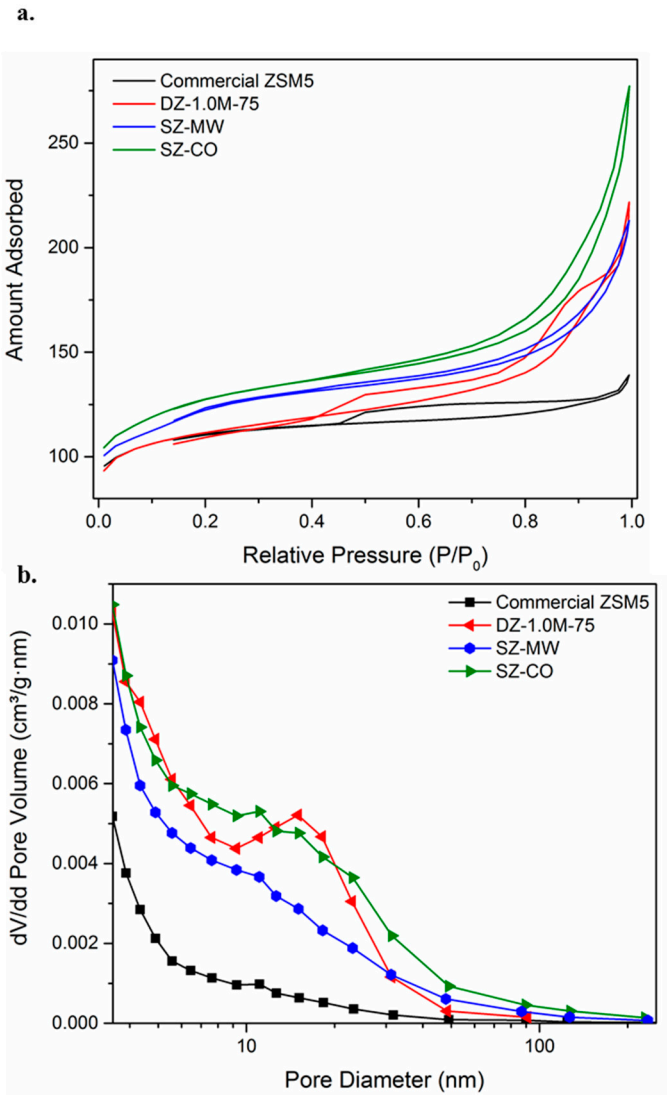

Figure 3. (**a**) N_2 isotherms and (**b**) pore size distributions for commercial and hierarchal ZSM-5 zeolites.

NH_3 TPD data plotted in Figure 4 (and Figure S4) show that a harsh treatment for DZ-1.0M-75 led to a decrease in the number of strong acid sites (350–500 °C region) with respect to pristine zeolite. Likewise, the two home-made ZSM-5 zeolites, namely SZ-CO and SZ-MW, exhibit a lower quantity of strong acid sites than the reference commercial catalyst (in line with results shown in Table 1). It is important to remind here that the H/D isotope exchange technique allows counting all exchangeable hydrons in the zeolites whatever their acidity, whilst the ammonia chemisorption experiment permits discrimination based on their acid strength. Based on the data collected in Table 1, it appears that these two complementary methods highlight the presence of more O-H groups in strongly desilicated samples, thus the presence of more silanol defects than bottom-up as obtained SZ-MW and SZ-CO zeolites. It can be assumed that the ZSM-5 zeolite series studied herein exhibits different textural properties (Figure 3) and especially rather distinct acid properties (Table 1, Figure 4).

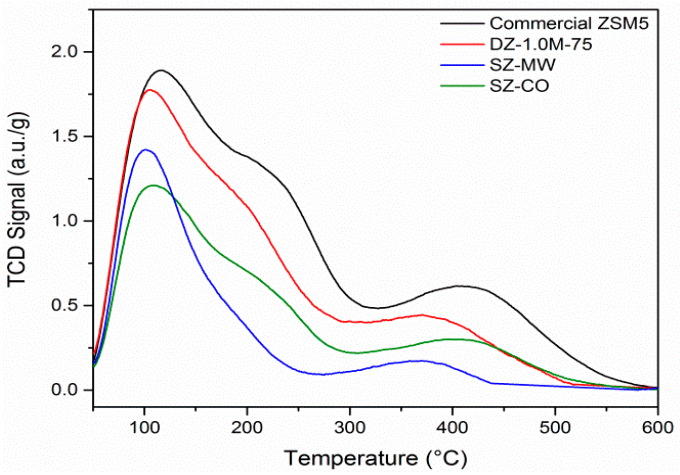

Figure 4. Ammonia thermally programmed desorption (NH_3 TPD) curves obtained for commercial and hierarchical ZSM-5 zeolites.

3. Catalysis

3.1. Diels Alder

The Diels Alder cyclisation reaction between isoprene and methylacrylate was used as a model reaction known to require only mild and medium acidity to achieve high yields in cycloadduct products (Table 2).

Table 2. Diels Alder reaction between isoprene and methylacrylate over the different zeolites.

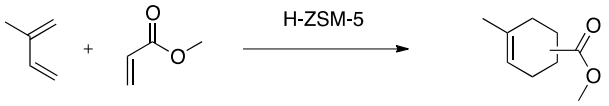

Entry	Zeolite	Conversion [%]	S(*Para*) [%]	TOF * 10^{-2} [h^{-1}]
1	CBV2314	97	90	14
2	DZ-0.2M-45	96	89	14
3	DZ-0.2M-75	95	92	28
4	DZ-0.2M-105	79	91	11
5	DZ-0.5M-45	75	92	23
6	DZ-1.0M-75	94	76	12
7 [a]	SiO_2/Al_2O_3	96	87	12

[a] amorphous silica alumina contains 1.31 mmol (H^+) g^{-1} and exhibits 100 m^2 g^{-1}.

It is noteworthy that mild desilication treatments led to considerable improvements in turnover frequencies (TOF); up to twice as high (entries 1 vs. 3), while maintaining a high selectivity towards the shape selectivity induced para product (Figure 5). In contrast, harsh treatments led to a decrease in TOF and a loss in micropores linked shape selectivity (entry 6). Interestingly, DZ-1.0M-75 (entry 6) behaved similarly to amorphous silica-alumina considering conversion and TOF values (entry 7), indicating that the reaction occurred in the mesopores rather than in microporous shape selective network, which might have been damaged in this sample. Additionally, this is in agreement with XRD data while comparing crystalline qualities of the different samples. The lower 'para' selectivity observed over DZ-1.0M-75 (entry 6, Table 2) might also be attributed to the presence of Al debris in the vicinity of BA sites, acting as Lewis acid sites, being able to guide the activation of the diene towards the formation of the 'ortho' cycloadduct. This observation is line with the similar trend of amorphous SiO_2/Al_2O_3 catalyst (entry 7, Table 2).

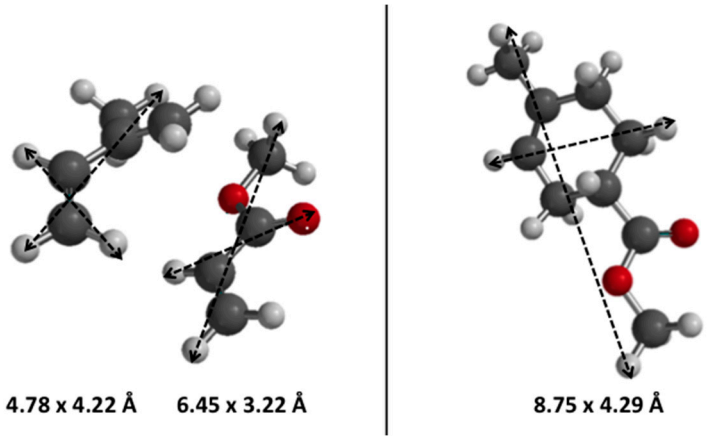

Figure 5. Molecular diameters of isoprene, methylacrylate and the main reaction product 1-carboxymethyl-4-methylcyclohex-3-ene.

The spectacular increase in TOF values achieved over DZ-0.2M-75 and DZ-0.5M-45 zeolites, from 14 up to 28 $\times$ 10^{-2} [h^{-1}], strongly suggests the favorable occurrence of the cycloaddition reaction within the microporous network. Indeed, DZ-0.2M-75 and DZ-0.5M-45 materials possess the highest internal surface areas among the top down desilicated samples.

Finally, one may also assume that this Diels Alder reaction can be used as a manner to compare the impact of the desilication treatment, i.e., duration versus alkaline medium concentration on the selectivity towards 'endo' product and in terms of turnover frequency.

3.2. Methanol-to-Hydrocarbons

The series of ZSM-5 zeolites were compared in the gas-solid Methanol-To-Olefins (MTO) reaction. It has to be mentioned that none of the tested Al-rich ZSM-5 zeolites can a priori be considered as a promising catalyst for this reaction. However, the conversion of methanol to hydrocarbons may give precious insights regarding the interconnectivity between micro- and mesopores. Indeed, we could observe that the most harshly treated samples exhibited higher selectivities towards the formation of light olefins (ethylene-propylene-butylenes) than pristine sample (Table 3). The parent zeolite (entry 1) exhibits a 42% selectivity towards C_2-C_4 light olefins, while for mildly and harshly treated samples (entries 2–5) this selectivity is close to (or above) 50%. In contrast, the two synthesised samples (entries 6 and 7) can be really considered as MTO catalysts with selectivities towards C_2-C_4 olefins approaching 60%.

Table 3. Conversion of methanol-to-hydrocarbons. Selectivities were given after Time on Stream (TOS) = 1 h once quasi-steady state was reached; 450 °C; Weight Hourly Space Velocity (WHSV) = 1.12 h^{-1}.

Entry	Zeolite	Conversion [%]	S(C_{1-4}) [%]	S($C_{2=}$) [%]	S($C_{3=}$) [%]	S($C_{4=}$) [%]	S($C_{5=}$) [%]	S(C_{6+}) [%]
1	CBV2314	100	23	11	25	6	7	27
2	DZ-0.2M-45	97	25	16	27	6	6	19
3	DZ-0.2M-75	87	27	21	29	3	3	17
4	DZ-0.2M-105	99	27	16	26		6	17
5	DZ-1M-75	100	26	16	27	6	6	19
6	SZ-MW	97	6	6	38	16	18	16
7	SZ-CO	99	20	18	32	7	8	15

Surprisingly, the SZ-MW sample led to a high selectivity (78%) towards ethylene, propylene, butylenes and pentenes. This catalyst produced by far the highest amount of pentenes (18%), propylene

(38%) and only few C_1-C_4 alkanes (6%). One may expect a similar behaviour of the SZ-CO sample (which exhibits even higher Si/Al), but that was not the case. Hence, considering such low hydrogen transfer indices (HTI), the mesoporous mildly acidic SZ-MW sample was the only MFI-catalyst (among tested samples) favoring the occurrence of an olefin-propagation-cracking regime. The latter material behaves therefore as a true MTO catalyst, whilst the rest of the series led to MTG typical product distribution. Only slight improvements in terms of selectivities in light olefins depending on the harshness of the desilication treatment could be conclusively observed.

Figure 6 presents the conversion profile as a function of time on stream for all catalysts. In line with aforementioned observations, SZ-MW catalyst demonstrated the highest stability with almost no drop in conversion during 22 h on stream. It is noteworthy that all desilicated samples exhibit a faster deactivation with respect to pristine CBV2314 zeolite. The introduction of mesoporosity seems therefore to alter the stability for the MTO reaction. This is probably due to the easy formation and growth of coke in the generated mesopores. Consecutive reactions are occurring, thus favouring hydrogen transfer reactions. Both the production of gasoline and C_1-C_4 alkanes are warranted over top-down prepared samples in line selectivity results (Table 3).

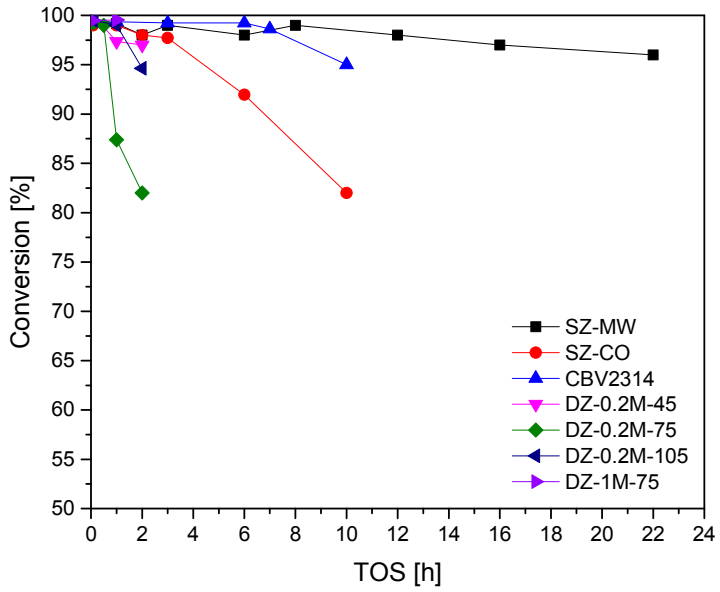

Figure 6. Methanol conversion into hydrocarbons profile versus TOS.

3.3. Chlorination of Iodobenzene

A third reaction was investigated, previously reported to be efficiently catalysed by various acidic zeolites in batch or semi-continuous gas-solid heterogeneous system [39,44,45].

Herein, the reaction has been carried out in a liquid–solid heterogeneous manner (Table 4). While the commercial zeolite led to a modest TOF and a para/ortho ratio of 1.4, these values could be substantially improved for mildly desilicated samples (entry 3) with a 50% relative increase in TOF and para/ortho ratio of 1.6.

Table 4. Liquid–solid chlorination reaction of iodobenzene with trichloroisocyanuric acid (TCCA) over different ZSM-5 zeolites.

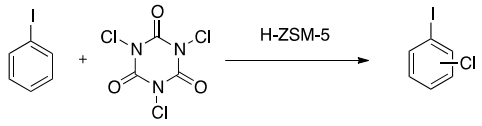

Entry	Zeolite	Conversion [%]	S(*Para*) [%]	S(*Ortho*) [%]	TOF [h^{-1}]
1	CBV2314	43	47	33	6.4
2	DZ-0.2M-45	52	47	34	5.2
3	DZ-0.2M-75	33	52	33	9.6
4	DZ-0.2M-105	48	52	36	5.2
5	DZ-0.5M-45	49	52	35	9.1
6	DZ-1.0M-75	52	52	36	8.7
7	SZ-MW	43	63	25	12.7
8	SZ-CO	61	52	35	11.7
9 [a]	H_2SO_4	80	44	44	5.4

[a] comparison to homogeneous catalysis: 8 µL H_2SO_4 corresponding to 0.148 mmol H^+.

It is important to mention here that para/ortho ratio gives an indication for the degree of micropores-linked shape selectivity that occurs during the iodobenzene chlorination reaction (the thermodynamic equilibrium being para/ortho = 1, entry 9). The two as-prepared SZ-MW and SZ-CO zeolites exhibited again the best catalytic performances reaching a twice as high TOF with respect to the commercial zeolite and a para/ortho ratio of 2.5 (entry 7). Figure 7 presents the molecular diameters of the reactants and two major products.

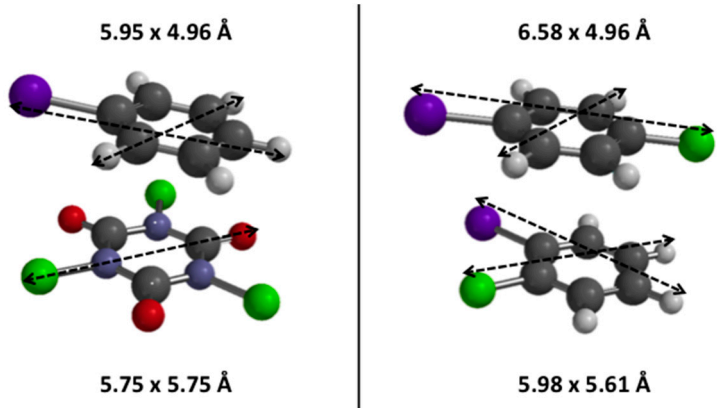

Figure 7. Molecular diameters of iodobenzene and TCCA and the two major products of this reaction, ortho- and para-chloroiodobenzene.

It is important to mention that the generation of mesopores either via desilication or via the constructive method led to the highest TOF values, thus confirming that enhanced internal diffusion favours the chlorination reaction. As a priori expected, a liquid–solid reaction involving rather bulky reagents might be hindered by internal mass transfer [39]. SZ-MW already proved to be the most promising MTO-catalyst. In this reaction, a proper connectivity between its meso- and microporosity led to the combined higher TOF and higher selectivity towards the shape selective product. This cheap and easy to set-up halogenation reaction hence seems to be a simple additional tool to evaluate pores-connectivity.

3.4. Friedel-Crafts Acylation of Anisole

The Friedel-Crafts acylation of anisole with two different carboxylic acids was also investigated, usually requiring a strong BrØnsted acid strength. The smaller propanoic acid is able to diffuse within the microporous network of ZSM-5 zeolites and, thus, its acylation reaction should occur in such shape selective environments. The opposite is expected for the larger heptanoic acid, which may barely react within the microporous network to form acylation products (Figure 8). In Table 5, it can be seen that DZ-0.2M-75 (entry 3) behaves as the best catalyst with a 50% relative improvement in TOF values with respect to pristine zeolite and, more interestingly, producing the main ortho-substituted product with a three times higher selectivity.

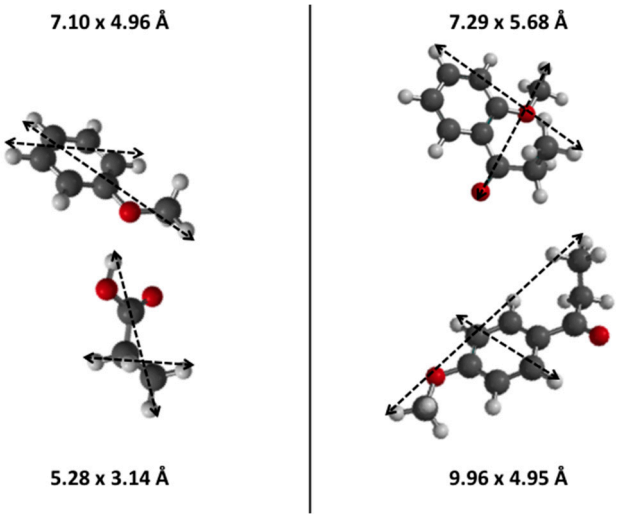

Figure 8. Molecular diameters of propanoic acid, anisole and the two major products: ortho- and para-substituted anisole.

Table 5. Friedel Crafts acylation of anisole with propionic acid over the different zeolites.

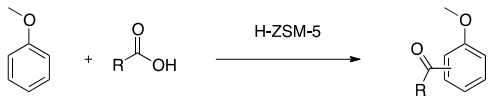

Entry	Zeolite	Conversion [%]	S(*Para*) [%]	S(*Ortho*) [%] [a]	TOF * 10^{-2} [h^{-1}]
1	CBV2314	75	15	26	27
2	DZ-0.2M-45	72	8	64	22
3	DZ-0.2M-75	64	8	67	40
4	DZ-0.2M-105	76	19	28	21
5	DZ-0.5M-45	62	13	40	38
6	DZ-1.0M-75	80	8	63	36
7	SZ-MW	73	23	43	53
8	SZ-CO	33	30	26	48
9	SiO_2/Al_2O_3	0	0	0	0
10 [b]	H_2SO_4	79	39	36	4

[a] byproducts are de-methylated anisole and Fries-rearrangement products; [b] 0.1 mL H_2SO_4 corresponding to 1.9 mmol H^+.

The degree of carboxylic acid conversion can be assumed nearly constant, only varying between 62–80% among all zeolites. The selectivity towards the ortho regioisomer increases with the extent of the desilication treatment, thus being favoured in the mesopores. This assumption is supported by the higher mesoporous volumes present in DZ-0.2M-75 and DZ-1.0M-75.

Again, it is important to mention that the highest TOF values were achieved over as-synthesised ZSM-5 zeolites (entries 7 and 8) with almost twice as high as parent zeolite. Amorphous silica-alumina

did not exhibit any catalytic activity, thus suggesting the preferential occurrence of the acylation reaction in the zeolite micropores. Besides, the creation of (probably) connected mesopores with micropores led to higher TOF values.

In contrast, the reaction performed with sulphuric acid (entry 10) led to a complete inversion in ortho/para regioisomers selectivity, corresponding to the thermodynamic equilibrium obtained under non-shape selective conditions.

The acylation with heptanoic acid has to be considered to be favoured either inside the mesoporous network or (perhaps) at the micropores pore-mouth entrances, which are in turn more present in mesoporous zeolites. Indeed, the TOF values could be quadrupled over mesoporous zeolites in mildly treated DZ-0.2M-75 while even a 5-times higher TOF could be measured for harsher treated DZ-0.5M-45 (entry 5, Table 6) with respect to parent zeolite. Again, the reaction catalysed by sulphuric acid indicates the thermodynamic equilibrium (entry 10).

Table 6. Friedel Crafts acylation or anisole with heptanoic acid over different zeolites.

Entry	Zeolite	Conversion [%]	S(*Para*) [%]	S(*Ortho*) [%] [a]	TOF * 10^{-2} [h^{-1}]
1	CBV2314	7	0	100	3
2	DZ-0.2M-45	21	34	19	6
3	DZ-0.2M-75	19	17	31	12
4	DZ-0.2M-105	13	54	46	4
5	DZ-0.5M-45	24	27	22	15
6	DZ-1.0M-75	21	25	49	8
7	SZ-MW	26	40	19	19
8	SZ-CO	9	58	42	13
9	SiO_2/Al_2O_3	0	0	0	0
10 [b]	H_2SO_4	55	10	37	3

[a] byproducts are Fries rearrangement products; [b] 0.1 mL H_2SO_4 corresponding to 1.9 mmol H^+.

The bottom-up designed SZ-MW (entry 7) exhibiting the highest TOF value of 19 is therefore interesting in terms of selectivity, since an inversion of the thermodynamically favoured product from ortho-, under non-shape selective conditions, to para- in shape selective micro/mesoporous zeolites could be observed (Figure 9).

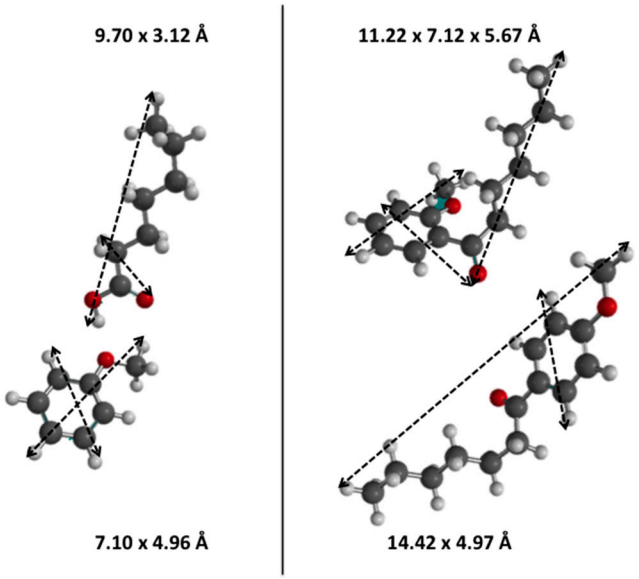

Figure 9. Molecular diameters of heptanoic acid, anisole and the two major products: the ortho- and para-substituted anisole.

Figure 10 aims to summarise all the catalytic results being expressed as TOF versus surface acid sites density. The H/D isotope exchange technique was used for the estimation of the total surface acidity since all hydrons (silanol groups, bridging Al-(OH)-Si) might be exchanged [46]. As desilication may create silanol defects, which can be either internal or external, the total BET surface area was chosen to express the surface Brønsted acid site density. The dependence between TOF values and BrØnsted surface acidity depends on the type of reaction chosen (Figure 10).

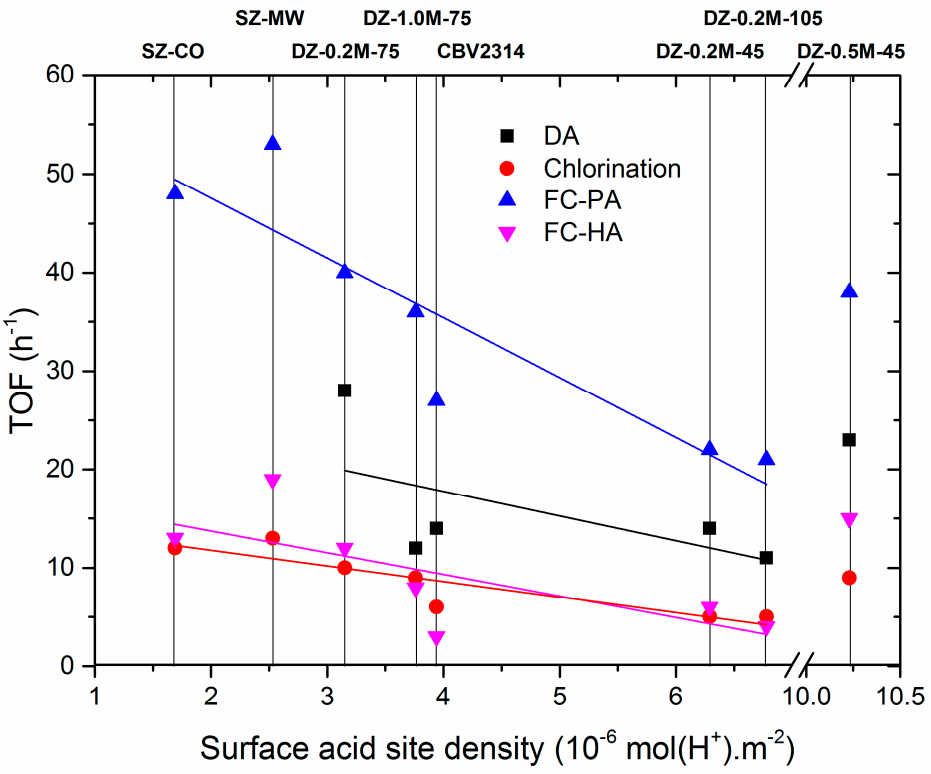

Figure 10. Tentative linear correlation between the turnover frequencies over the different zeolites in the catalytic applications (DA: Diels-Alder cyclization, Chlorination of iodobenzene, FC-PA: Friedel-Crafts acylation of anisole with propionic acid, and FC-HA: Friedel-Crafts acylation of anisole with heptanoic acid) and their respective calculated surface acid site densities (calculated using total exchangeable hydrons, determined by H/D-isotope exchange technique, and the total Brunauer-Emmet-Teller (BET) surface area).

The model reactions, which probably occurred within the microporous network, i.e., the chlorination of iodobenzene and the Friedel-Crafts acylation of anisole with propionic acid follow a tight linear fit. Hence, these highly acid strength-demanding reactions are favoured over ZSM-5 zeolites possessing more isolated Brønsted acid sites.

In contrast, for Diels-Alder cyclisation this linear relationship seems more volatile. Likewise, the Friedel-Crafts acylation of anisole with heptanoic acid seems more affected by the presence of mesopores rather than surface acidity. It is noteworthy that the slope of the Friedel-Crafts acylation of anisole with heptanoic acid (FC-HA) fit is much smaller than the slope of Friedel-Crafts acylation of anisole with propionic acid (FC-PA), thus indicating a greater impact for the latter involvement of micropores in the catalysed reaction.

Likewise, the microporous network appears as a governing parameter for the methanol conversion into hydrocarbons in terms of selectivity towards light olefins (Figure 11). The higher the acid site dispersion is, the higher the selectivity towards C_2-C_4 olefins is.

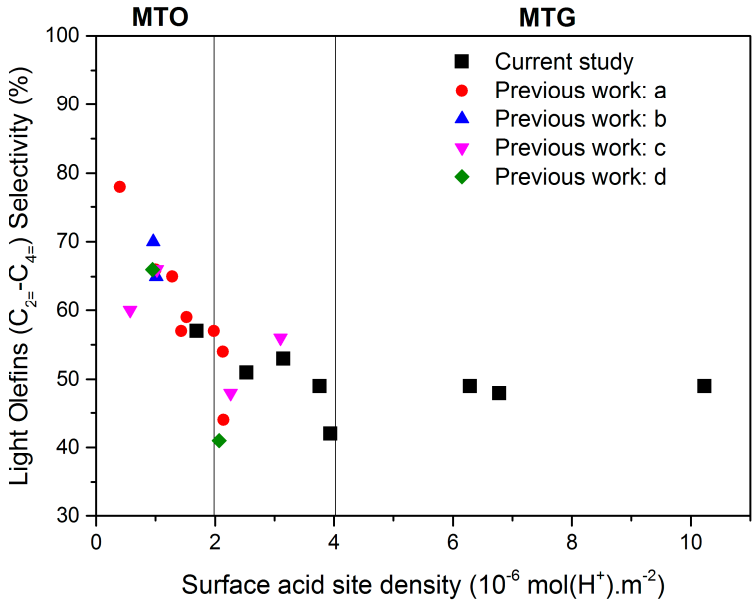

Figure 11. Hyperbolic correlation between light olefins selectivity over tested ZSM-5 zeolites and their respective calculated surface acid site densities (calculated using their total exchangeable hydrons, obtained by H/D-isotope exchange technique, and the total BET surface area). (a) Reported in [47] (b) [48] (c) [40] and (d) [49].

The presence of higher surface acid density induces a drop in C_2-C_4 olefins selectivity, from 80% [47] to below 50% as reported herein. Indeed, the more the acid sites, the more consecutive reactions are occurring, thus favouring hydrogen transfer reactions hence both the production of gasoline and C_1-C_4 alkanes.

The bottom-up synthesised mesoporous (SZ-MW and SZ-CO) samples behave in most cases better than top-down as-prepared catalysts. This can be explained by a higher crystallinity with respect to desilicated zeolites that exhibit a loss in crystal quality. Besides, a higher Si/Al ratio is also observed for the former two zeolites, thus suggesting a better resistance to deactivation by coking. Among SZ-MW and SZ-CO, the latter exhibits a higher Si/Al ratio that underlines the impact of possessing more disperse acid sites which positively impacts its reactivity in MTO. In contrast, SZ-MW (with more acid sites) allows achieving a higher conversion in FC reaction.

By properly selecting the desilication treatment (duration, concentration, temperature) or the constructive approach to introduce mesoporosity, it is possible to design an optimal acid catalyst depending on the targeted catalytic reaction. The herein presented cheap catalytic reactions are sensitive tools for qualitatively characterising meso- and micropores connectivity.

4. Experimental Section

4.1. Zeolites

The commercial zeolite was purchased from Zeolyst International (SiO_2/Al_2O_3 = 23, CBV2314). All samples were calcined in air at 550 °C for 10 h before catalytic testing. Nanocrystalline zeolites were synthesised according to the recipe previously reported by Petushkov et al. [50]. In summary, the gel having the following mole composition was prepared: 25 TEOS:1 $NaAlO_2$:5 TPAOH:4 TPABr:1000 H_2O, where TPAOH = tetra-n-propylammonium hydroxide (Alfa Aesar, Ward Hill, MA, USA, 40%), TPABr = tetra-n-propylammonium bromide (Sigma-Aldrich, St. Louis, MO, USA, 98%), and TEOS = tetraethyl orthosilicate (Aldrich, St. Louis, MO, USA, 98%). One third of the water, TPAOH, and sodium aluminate (Strem Chemicals, Newburyport, MA, USA, 99.9%) were mixed and vigorously stirred for 5 min. The remaining water and template TPABr were then added to the mixture and

stirred for 5 min. Finally, TEOS was poured in the solution and stirred overnight at room temperature in a closed polypropylene reactor. The gel was loaded in a Teflon-lined autoclave. Oven synthesis (SZ-CO) occurred in a Parr stainless steel autoclave (Parr 4744) placed in the middle of a pre-heated mechanical convection oven (Thermo Scientific Heratherm OMS100, Waltham, MA, USA) at 150 °C for 24 h. The microwave synthesised sample (SZ-MW) was loaded into a Mars 6 EasyPrep vessel with fibre optic temperature probe and heated using a CEM Mars 6 microwave at 150 °C for 5 h. After the synthesis, the powders were collected by centrifugation (5000 rpm, 30 min) and washed twice with deionised water and ethanol. The slurry was subsequently dried at 70 °C overnight and then calcined at 550 °C for 10 h to decompose the TPA. Finally, the acid form of ZSM-5 was obtained after three cationic exchanges with a 0.5 M NH_4NO_3 (Fisher Scientific, Pittsburgh, PA, USA, ACS) solution at 70 °C, drying at 70 °C overnight, and calcination at 550 °C for 10 h.

4.2. Post-Synthetic Modifications

First, 2 g of commercial zeolite were placed in a 50 mL sodium hydroxide (Pellets, Fischer Scientific, 99.2%) solution at concentrations of 0.2 M, 0.5 M, and 1.0 M in a 125 mL Nalgene bottle. The bottle was immerged in a pre-heated oil bath at 65 °C for 45, 75, or 105 min under vigorous stirring. The sample was then placed in an ice bath for 10 min to quench the reaction. Solutions were centrifuged and the liquid phase decanted. The zeolite was then washed with deionised water to obtain a pH $\leq$ 9. After, 50 mL of 0.1 M HCl was added to the zeolite to remove extra-framework aluminium (EFAl). The solution was vigorously stirred in an oil bath at 65 °C for 4 h. The zeolite was then washed with deionised water three times to obtain a pH $\geq$ 5. Following the final rinse, the zeolite was ion exchanged three times with 100 mL of 0.2 M ammonium nitrate solution. The sample was then calcined at 550 °C for 10 h with a 5° min^{-1} ramp to produce the H-form catalyst. Table S1 summarizes the denomination of zeolites under investigation.

4.3. Characterisation

The crystallinity of as-prepared materials was analysed by powder X-ray diffraction (XRD) using a Cu X-ray tube (λ = 0.15418 nm) on a Siemens D500 X-ray diffractometer. The powder patterns were collected at room temperature in the $5 < 2\theta < 50°$ range with a 2θ angle step of 0.05° and a 3 s dwell time. All data were processed using Jade software (V9.5, Christchurch, New Zealand). Test specimens were prepared by mixing the zeolite sample with an internal standard (high purity corundum, Alpha Aesar, verified using NIST 674b standards). The mixture consisted of 40% internal standard by mass. A thin film analysis was performed on the 1.0 M treated sample due to the small amount of zeolite remaining post synthesis.

Sample topography and particle size were investigated by SEM. Images were acquired with a FEI Quanta FEG 250 operated at 10 kV. Elemental composition was determined using energy dispersive X-ray spectroscopy (EDS) on an Oxford Instruments Aztec™ spectrometer system equipped with an X-Max 80 detector. SEM images and EDS spectra were acquired with accelerating voltages of 10 kV and 15 kV, respectively.

Micromeritics ASAP 2020 system was used for nitrogen adsorption-desorption measurements at 77 K. Prior to analysis, zeolite powder (50 mg) was outgassed for 12 h at 200 °C under vacuum (10 μm Hg). Specific surface areas were determined from the Brunauer-Emmet-Teller (BET) equation. Pore size distributions were calculated from the adsorption branch of the isotherm using the Barret-Joyner-Halenda (BJH) model with Faas correction. The *t*-plot method was used to distinguish micropores from mesopores.

Temperature programmed desorption of ammonia (NH_3-TPD) was performed using a Micromeritics Autochem II 2920. Zeolite powder (50 mg) was pre-treated at 550 °C in He for 1 h to desorb moisture from the surface. The sample was then cooled to 50 °C and ammonia adsorbed for 30 min (20 mL min^{-1} of 10 vol % NH_3 in He). The sample was purged at 100 °C under He flow for

90 min. NH_3 desorption was recorded by heating the zeolite from 100 to 700 °C and the curves were normalised using sample mass.

Acid site densities were also determined by H/D isotope exchange method as reported elsewhere [51].

4.4. Catalytic Tests

Molecular dimensions of substrates and products of the various investigated reactions were estimated using Spartan software (Irvine, CA, USA).

4.4.1. Diels Alder

The procedure is described elsewhere [37]. Catalytic experiments were performed at iso-Brønsted acid site conditions by changing the mass of the catalyst. Under Ar atmosphere, zeolite (551 mg, activated at 550 °C during 15 h), was placed in dry heptane (3 mL; or dry cyclohexane) under stirring at room temperature. Methyl acrylate (0.375 mL) in dry heptane (2 mL; or dry cyclohexane) was added to the mixture. Finally, isoprene (0.25 mL) was added separately and the mixture was stirred at 75 °C for 24 h. The catalyst was then isolated by filtration over a Millipore membrane and the filtrate was analysed by gas chromatography GC (HP5890 Series II, Pona column, 50 m) equipped with a flame ionisation detector (FID).

4.4.2. Methanol-to-Hydrocarbons

Prior to use, catalysts were calcined at 550 °C with a gradient of 15 °C min^{-1} in static air as it has been reported elsewhere [38]. H-zeolites were sieved and particles <250 μm were used in the catalytic tests. Then, 60 mg of zeolite were introduced in a tubular quartz reactor, packed between quartz wool plugs. A methanol-saturated nitrogen-flow was fed to the reactor at 450 °C (WHSV = 1.12 $g_{MeOH}/(g_{cat}\ h)^{-1}$). Samples withdrawn at the reactor outlet were analysed by GC (HP5890 Series II, Pona column, 50 m). The activity of the catalysts was expressed in terms of methanol and dimethylether conversion.

4.4.3. Chlorination of Iodobenzene

This halogenation reaction was carried out following the same procedure as recently reported [52]. Catalytic reactions were done in 5 mL dichloroethane, to which iodobenzene (1 mmol, 0.112 mL, 1 equiv.), TCCA (0.34 mmol, 0.079 g, 0.34 equiv.) and the respective catalysts (100 mg) were added (at iso-mass conditions). The solution was stirred at 80 °C and 500 rpm velocity for 1 h. The samples withdrawn for GC analysis (0.1 mL) were filtered over a celite filled cartridge with 2 mL CH_2Cl_2 and vigorously stirred with 3 mL of a 10 wt %. $Na_2S_2O_3$ solution. From the resulting biphasic solution, the organic layer was separated and dried over Na_2SO_4 and finally injected in the gas chromatograph (GC 5890 Hewlett Packard) equipped with a capillary column (PONA, 50 m) and a flame ionisation detector (FID). In principle, the chlorination of iodobenzene leads to mono-, di- or tri-substituted aromatics. Para- and ortho-substituted aromatics are favored. The degree of conversion and the selectivity towards the different products were calculated by taking into account the response factor of iodobenzene reactant and those from the products (mono-, di- and tri-chlorinated aromatics) through the use of an external standard (n-heptane). Blank experiments were carried out; without catalyst and one homogeneously catalysed reaction with sulphuric acid and used at iso-site conditions with respect to 100 mg H-ZSM-5 CBV2314 (0.148 mmol H^+) which corresponds to 8 μL H_2SO_4.

4.5. Friedel-Crafts Acylation of Anisole

Based on the studies of Kantam et al. [53] and Wang et al. [54], which demonstrated better catalytic performance while using aromatic substrates as solvents, we decided to carry out the reaction in a sealed tube where solid acid (250 mg), then anisole placed on molecular sieve (10 mmol, Sigma-Aldrich)

and carboxylic acid (2.5 mmol, propanoic acid, Sigma-Aldrich, or heptanoic acid Alfa Aesar) were mixed together at 150 °C for 24 h. Then, the crude was filtered on a Nylon Millipore membrane with $CDCl_3$ as filtration solvent and analysed by ^1H NMR (Bruker Advance 300 MHz).

5. Conclusions

ZSM-5 zeolites were modified by various desilication post-treatments with NaOH solution, and compared to two mesopores-containing home-made zeolites. Indeed, three liquid–solid and one gas–solid reactions were chosen to successfully build relationships between zeolites textural properties and their behaviour in acid-catalysed reactions: Diels-Alder cyclisation between isoprene and methylacrylate, methanol conversion into hydrocarbons, chlorination of iodobenzene with TCCA, Friedel-Crafts acylation of anisole by propionic or heptanoic acids.

The cheap creation of mesoporosity via desilication proved beneficial in each of the studied reactions (higher TOF values), while the respective product distributions were found to be an interesting qualitative indication for the shape selective micropores-accessibility. In other terms, these reactions could be used to characterise the micro-mesopores connectivity.

Depending on the catalytic application chosen, an optimal treatment has to be set to achieve high activity and selectivity. For example, it turned out that the strong acidity-demanding acylation reaction is preferably conducted over catalysts with low surface acid site densities. This electrophilic aromatic substitution reaction, via its shape selectivity-impacted product distribution, proved to be a valuable tool to assess the micropores-accessibility.

Supplementary Materials: The following are available online at www.mdpi.com/2073-4344/7/8/225/s1, Figure S1: Powder XRD patterns obtained for (A) commercial and hierarchical zeolites (B) scaled to the most intense characteristic MFI peaks, Figure S2: SEM images of NaOH desilicated ZSM-5 treated with (A) 0.2 M NaOH for 45 min, (B) 0.2 M NaOH for 75 min, (C) 0.2 M NaOH for 105 min, and (D) 0.5 M, 75 min, Figure S3: (A) N_2 isotherms and (B) pore size distributions for commercial and hierarchical ZSM-5 zeolites, Figure S4: Ammonia temperature programmed desorption curves obtained for commercial and hierarchical ZSM-5 zeolites, Table S1: Denomination of zeolites under investigation, Table S2: Microporous and mesoporous volumes of the different zeolites.

Acknowledgments: P.L. is thankful to the National Research Fund of Luxembourg (NRFL) for his PhD-grant (5898454).

Author Contributions: J.P.T. and B.L. conceived and designed the experiments; P.L., J.F.K., T.C.H., C.B. performed the experiments; P.L., B.L., T.C.H. and J.P.T. analyzed the data and wrote the paper.

Conflicts of Interest: The authors declare no conflict of interest.

References

1. Pérez-Ramírez, J.; Christensen, C.H.; Egeblad, K.; Christensen, C.H.; Groen, J.C. Hierarchical zeolites: enhanced utilisation of microporous crystals in catalysis by advances in materials design. *Chem. Soc. Rev.* **2008**, *37*, 2530–2542. [CrossRef] [PubMed]
2. Serrano, D.P.; Aguado, J.; Morales, G.; Rodriguez, J.M.; Peral, A.; Thommes, M.; Epping, J.D.; Chmelka, B.F. Molecular and Meso- and Macroscopic Properties of Hierarchical Nanocrystalline ZSM-5 Zeolite Prepared by Seed Silanization. *Chem. Mater.* **2009**, *21*, 641–654. [CrossRef]
3. Serrano, D.P.; Garcia, R.A.; Vicente, G.; Linares, M.; Prochazkova, D.; Cejka, J. Acidic and catalytic properties of hierarchical zeolites and hybrid ordered mesoporous materials assembled from MFI protozeolitic units. *J. Catal.* **2011**, *279*, 366–380. [CrossRef]
4. Xin, H.; Koekkoek, A.; Yang, Q.; van Santen, R.; Li, C.; Hensen, E.J.M. A hierarchical Fe/ZSM-5 zeolite with superior catalytic performance for benzene hydroxylation to phenol. *Chem. Commun.* **2009**, 7590–7592. [CrossRef] [PubMed]
5. Thibault-Starzyk, F.; Stan, I.; Abelló, S.; Bonilla, A.; Thomas, K.; Fernandez, C.; Gilson, J.P.; Pérez-Ramírez, J. Quantification of enhanced acid site accessibility in hierarchical zeolites—The accessibility index. *J. Catal.* **2009**, *264*, 11–14. [CrossRef]

6. Groen, J.C.; Zhu, W.; Brouwer, S.; Huynink, S.J.; Kapteijn, F.; Moulijn, J.A.; Pérez-Ramírez, J. Direct demonstration of enhanced diffusion in mesoporous ZSM-5 zeolite obtained via controlled desilication. *J. Am. Chem. Soc.* **2007**, *129*, 355–360. [CrossRef] [PubMed]
7. Li, X.; Prins, R.; van Bokhoven, J.A. Synthesis and characterization of mesoporous mordenite. *J. Catal.* **2009**, *262*, 257–265. [CrossRef]
8. Wei, X.; Smirniotis, P.G. Development and characterization of mesoporosity in ZSM-12 by desilication. *Microporous Mesoporous Mater.* **2006**, *97*, 97–106. [CrossRef]
9. Caicedo-Realpe, R.; Pérez-Ramírez, J. Mesoporous ZSM-5 zeolites prepared by a two-step route comprising sodium aluminate and acid treatments. *Microporous Mesoporous Mater.* **2010**, *128*, 91–100. [CrossRef]
10. Milina, M.; Mitchell, S.; Cooke, D.; Crivelli, P.; Pérez-Ramírez, J. Impact of pore connectivity in the design of long-lived zeolite catalysts. *Angew. Chem. Int. Ed. Engl.* **2015**, *54*, 1591–1594. [CrossRef] [PubMed]
11. Gueudré, L.; Milina, M.; Mitchell, M.; Pérez-Ramírez, J. Superior mass transfer properties of technical zeolite bodies with hierarchical porosity. *Adv. Funct. Mater.* **2014**, *24*, 209–219. [CrossRef]
12. Schneider, D.; Mehlhorn, D.; Zeigermann, P.; Kärger, J.; Valiullin, R. Transport properties of hierarchical micro–mesoporous materials. *Chem. Soc. Rev.* **2016**, *45*, 3439–3467. [CrossRef] [PubMed]
13. Milina, M.; Mitchell, S.; Crivelli, P.; Cooke, D.; Pérez-Ramírez, J. Mesopore quality determines the lifetime of hierarchically-structured zeolite catalysts. *Nat. Commun.* **2014**, 1–10. [CrossRef]
14. Aguado, J.; Serrano, D.P.; Rodriguez, J.M. Zeolite Beta with hierarchical porosity prepared from organofunctionalized seeds. *Microporous Mesoporous Mater.* **2008**, *115*, 504–513. [CrossRef]
15. Tao, Y.; Kanoh, H.; Abrams, L.; Kaneko, K. Mesopore-Modified zeolites: Preparation, characterization and applications. *Chem. Rev.* **2006**, *106*, 896–910. [CrossRef] [PubMed]
16. Egeblad, K.; Christensen, C.H.; Kustova, M.; Christensen, C.H. Templating mesoporous zeolites. *Chem. Mater.* **2008**, *20*, 946–960. [CrossRef]
17. Losch, P.; Boltz, M.; Soukup, K.; Song, I.H.; Yun, H.S.; Louis, B. Binderless Zeolite Coatings on Macroporous α-SiC Foams. *Microporous Mesoporous Mater.* **2014**, *188*, 99–107. [CrossRef]
18. Zhang, X.; Liu, D.; Xu, D.; Asahina, S.; Cychosz, K.A.; Agrawal, K.V.; Wahedi, Y.A.; Bhan, A.; Hashimi, S.A.; Terasaki, O. Synthesis of self-pillared zeolite nanosheets by repetitive branching. *Science* **2012**, *336*, 1684–1687. [CrossRef] [PubMed]
19. Mishnaevsky, L.; Tsapatsis, M. Hierarchical materials: Background and perspectives. *MRS Bull.* **2016**, *41*, 661–666. [CrossRef]
20. Keoh, S.H.; Chaikittisilp, W.; Muraoka, K.; Mukti, R.R.; Shimojima, A.; Kumar, P.; Tsapatsis, M.; Okubo, T. Factors Governing the Formation of Hierarchically and Sequentially Intergrown MFI Zeolites by Using Simple Diquaternary Ammonium Structure-Directing Agents. *Chem. Mater.* **2016**, *28*, 8997–9007. [CrossRef]
21. Yamada, H.; Iida, T.; Liu, Z.; Naraki, Y.; Ohara, K.; Kohara, S.; Okubo, T.; Wakihara, T. Downsizing AFX Zeolite Crystals to Nanoscale by a Postmilling Recrystallization Method. *Cryst. Growth Des.* **2016**, *16*, 3389–3394. [CrossRef]
22. Beyer, H.K. *Molecular Sieves: Science and Engineering*; Karge, H.G., Weitkamp, J., Eds.; Springer: Berlin/Heidelberg, Germany, 2002; Volume 3, pp. 203–255.
23. Groen, J.C.; Moulijn, J.A.; Pérez-Ramírez, J. Desilication: On the controlled generation of mesoporosity in MFI zeolites. *J. Mater. Chem.* **2006**, *16*, 2121–2131. [CrossRef]
24. Groen, J.C.; Moulijn, J.A.; Pérez-Ramírez, J. Alkaline post-treatment of MFI zeolites. From accelerated screening to scale-up. *Ind. Eng. Chem. Res.* **2007**, *46*, 4193–4201. [CrossRef]
25. Zhou, Q.; Wang, Y.-Z.; Tang, C.; Zhang, Y.-H. Modifications of ZSM-5 zeolites and their applications in catalytic degradation of LDPE. *Polym. Degrad. Stab.* **2003**, *80*, 23–30. [CrossRef]
26. Holm, M.S.; Hansen, M.K.; Christensen, C.H. "One-Pot" Ion-Exchange and Mesopore Formation during Desilication. *Eur. J. Inorg. Chem.* **2009**, 1194–1198. [CrossRef]
27. Abelló, S.; Bonilla, A.; Pérez-Ramírez, J. Mesoporous ZSM-5 zeolite catalysts prepared by desilication with organic hydroxides and comparison with NaOH leaching. *Appl. Catal. A* **2009**, *364*, 191–198. [CrossRef]
28. Ahn, J.H.; Kolvenbach, R.; Al-Khattaf, S.S.; Jentys, A.; Lercher, J.A. Enhancing shape selectivity without loss of activity—Novel mesostructured ZSM5 catalysts for methylation of toluene to *p*-xylene. *Chem. Commun.* **2013**, *49*, 10584–10586. [CrossRef] [PubMed]
29. You, S.J.; Park, E.D. Effects of dealumination and desilication of H-ZSM-5 on xylose dehydration. *Microporous Mesoporous Mater.* **2013**, *186*, 121–129. [CrossRef]

30. Silaghi, M.; Chizallet, C.; Raybaud, P. Challenges on molecular aspects of dealumination and desilication of zeolites. *Microporous Mesoporous Mater.* **2014**, *191*, 82–96. [CrossRef]
31. Groen, J.C.; Jansen, J.C.; Moulijn, J.A.; Pérez-Ramírez, J. Optimal aluminium-assisted mesoporosity development in MFI zeolites by desilication. *J. Phys. Chem. B* **2004**, *108*, 13062–13065. [CrossRef]
32. Chal, R.; Gerardin, C.; Bulut, M.; van Donk, S. Overview and Industrial Assessment of Synthesis Strategies towards Zeolites with Mesopores. *ChemCatChem* **2011**, *3*, 67–81. [CrossRef]
33. Chen, L.H.; Li, X.Y.; Rooke, J.C.; Zhang, Y.H.; Yang, X.Y.; Tang, Y.; Xiao, F.S.; Su, B.L. Hierarchically structured zeolites: Synthesis, mass transport properties and applications. *J. Mater. Chem.* **2012**, *22*, 17381–17403. [CrossRef]
34. Choi, M.; Na, K.; Kim, J.; Sakamoto, Y.; Terasaki, O.; Ryoo, R. Stable single-unit-cell nanosheets of zeolite MFI as active and long-lived catalysts. *Nature* **2009**, *461*, 246–249. [CrossRef] [PubMed]
35. Louis, B.; Gomes, E.S.; Coelho, T.; Lutzweiler, G.; Losch, P.; Silva, A.V.; Faro, A.C.; Romero, T.; Osman, M.B.; Balanqueux, A.; et al. Influence of Biomass Residues on the Metastability of Zeolite Structures. *Nanosci. Nanotechnol. Lett.* **2016**, *8*, 917–924. [CrossRef]
36. Silva, A.V.; Miranda, L.S.M.; Nele, M.; Louis, B.; Pereira, M.M. Insights to Achieve a Better Control of Silicon-Aluminum Ratio and ZSM-5 Zeolite Crystal Morphology through the Assistance of Biomass. *Catalysts* **2016**, *6*, 30. [CrossRef]
37. Bernardon, C.; Louis, B.; Bénéteau, V.; Pale, P. Diels–Alder Reaction between Isoprene and Methyl Acrylate over Different Zeolites: Influence of Pore Topology and Acidity. *ChemPlusChem* **2013**, *78*, 1134–1141. [CrossRef]
38. Losch, P.; Pinar, A.B.; Willinger, M.G.; Soukup, K.; Chavan, S.; Vincent, B.; Pale, P.; Louis, B. H-ZSM-5 Zeolite Model Crystals: Structure-Diffusion-Activity Relationship in Methanol-To-Olefins Catalysis. *J. Catal.* **2017**, *345*, 11–23. [CrossRef]
39. Boltz, M.; Losch, P.; Louis, B.; Rioland, G.; Tzanis, L.; Daou, T.J. MFI-type Zeolite Nanosheets for Gas-Phase Aromatics Chlorination: A Strategy to Overcome Mass Transfer Limitations. *RSC Adv.* **2014**, *4*, 27242–27249. [CrossRef]
40. Bleken, F.L.; Chavan, S.; Olsbye, U.; Boltz, M.; Ocampo, F.; Louis, B. Conversion of Methanol into light olefins over ZSM-5 zeolite: Strategy to enhance propene selectivity. *Appl. Catal. A* **2012**, *447–448*, 178–185. [CrossRef]
41. Daou, T.J.; Boltz, M.; Tzanis, L.; Michelin, L.; Louis, B. Gas-phase chlorination of aromatics over FAU- and EMT-type zeolites. *Catal. Commun.* **2013**, *39*, 10–13. [CrossRef]
42. Gomes, E.S.; Lutzweiler, G.; Losch, P.; Silva, A.V.; Bernardon, C.; Parkhomenko, K.; Pereira, M.M.; Louis, B. Strategy to design zeolite catalysts in the presence of biomass. *Microporous Mesoporous Mater.* **2017**, in press. [CrossRef]
43. Hoff, T.C.; Gardner, D.W.; Thilakaratne, R.; Wang, K.; Hansen, T.W.; Brown, R.C.; Tessonnier, J.P. Tailoring ZSM-5 Zeolites for the Fast Pyrolysis of Biomass to Aromatic Hydrocarbons. *ChemSusChem* **2016**, *9*, 1473–1482. [CrossRef] [PubMed]
44. Boltz, M.; de Mattos, M.C.S.; Esteves, P.M.; Pale, P.; Louis, B. Green route for the chlorination of nitrobenzene. *Appl. Catal. A* **2012**, *449*, 1–8. [CrossRef]
45. Losch, P.; Pascual, A.M.; Boltz, M.; Ivanova, S.; Louis, B.; Montilla, F.; Odriozola, J.A. Ionic liquid immobilization on carbon nanofibers and zeolites: Catalyst design for the liquid-phase toluene chlorination. *CR Chim.* **2015**, *18*, 324–329. [CrossRef]
46. Louis, B.; Vicente, A.; Fernandez, C.; Valtchev, V. Crystal Size Acid Sites Relationship Study of Nano- and Micrometer-Sized Zeolite Crystals. *J. Phys. Chem. C* **2011**, *115*, 18603–18610. [CrossRef]
47. Losch, P.; Boltz, M.; Bernardon, C.; Louis, B.; Palčić, A.; Valtchev, V. Impact of external surface passivation of nano-ZSM-5 in the Methanol-To-Olefins reaction. *Appl. Catal. A* **2016**, *509*, 30–37. [CrossRef]
48. Losch, P.; Laugel, G.; Martinez-Espin, J.S.; Chavan, S.; Olsbye, U.; Louis, B. Phosphorous Modified ZSM-5 Zeolites: Impact on Methanol Conversion into Olefins. *Top. Catal.* **2015**, *58*, 826–832. [CrossRef]
49. Missengue, R.N.M.; Losch, P.; Sedres, G.; Musyoka, N.M.; Fatoba, O.O.; Louis, B.; Pale, P.; Petrik, L.F. Transformation of South African coal fly ash into ZSM-5 zeolite and its application as an MTO catalyst. *Comptes Rendus Chim.* **2017**, *20*, 78–86. [CrossRef]
50. Petushkov, A.; Yoon, S.; Larsen, S.C. Synthesis of hierarchical nanocrystalline ZSM-5 with controlled particle size and mesoporosity. *Microporous Mesoporous Mater.* **2011**, *137*, 92–100. [CrossRef]

51. Louis, B.; Walspurger, S.; Sommer, J. Quantitative determination of Bronsted acid sites on zeolites: A new approach towards the chemical composition of zeolites. *Catal. Lett.* **2004**, *93*, 81–84. [CrossRef]
52. Losch, P.; Kolb, J.F.; Astafan, A.; Daou, J.T.; Pinard, L.; Pale, P.; Louis, B. Eco-compatible zeolite-catalysed continuous halogenation of aromatics. *Green Chem.* **2016**, *18*, 4714–4724. [CrossRef]
53. Kantam, M.L.; Ranganath, K.V.S.; Sateesh, M.; Kumar, K.B.S.; Choudary, B.M. Friedel–Crafts acylation of aromatics and heteroaromatics by beta zeolite. *J. Mol. Catal. A* **2005**, *225*, 15–20. [CrossRef]
54. Wang, Q.L.; Ma, Y.; Ji, X.; Yan, H.; Qiu, Q. Regioselective acylation of anisole with carboxylic acids over HZSM-5 catalyst. *J. Chem. Soc. Chem. Commun.* **1995**, 2307–2308. [CrossRef]